jth

ORIGINAL ARTICLE

Disulfide bond reduction and exchange in C4 domain of von Willebrand factor undermines platelet binding

Fabian Kutzki[1] | Diego Butera[2] | Angelina J. Lay[2] | Denis Maag[3] | Joyce Chiu[2] | Heng-Giap Woon[2] | Tomáš Kubař[3] | Marcus Elstner[3] | Camilo Aponte-Santamaría[1] | Philip J. Hogg[2] | Frauke Gräter[1,4]

[1]Heidelberg Institute for Theoretical Studies, Schloß-Wolfsbrunnenweg 35, Heidelberg, Germany

[2]The Centenary Institute, University of Sydney, Camperdown, NSW, 2050, Australia

[3]Institute of Physical Chemistry, Karlsruhe Institute of Technology, 76131 Karlsruhe, Germany

[4]University of Heidelberg, Im Neuenheimer Feld 205, Heidelberg, Germany

Correspondence
Camilo Aponte-Santamaría, Schloss-Wolfsbrunnenweg 35, 69118 Heidelberg, Germany.
Email: camilo.aponte@h-its.org

Philip J. Hogg, Building 93, Royal Prince Alfred Hospital, Missenden Rd, Camperdown NSW 2050 Australia.
Email: phil.hogg@sydney.edu.au

Frauke Gräter, Schloss-Wolfsbrunnenweg 35, 69118 Heidelberg, Germany.
Email: frauke.graeter@h-its.org

Abstract

Background: The von Willebrand factor (VWF) is a key player in regulating hemostasis through adhesion of platelets to sites of vascular injury. It is a large, multi-domain, mechano-sensitive protein that is stabilized by a net of disulfide bridges. Binding to platelet integrin is achieved by the VWF-C4 domain, which exhibits a fixed fold, even under conditions of severe mechanical stress, but only if critical internal disulfide bonds are closed.

Objective: To determine the oxidation state of disulfide bridges in the C4 domain of VWF and implications for VWF's platelet binding function.

Methods: We combined classical molecular dynamics and quantum mechanical simulations, mass spectrometry, site-directed mutagenesis, and platelet binding assays.

Results: We show that 2 disulfide bonds in the VWF-C4 domain, namely the 2 major force-bearing ones, are partially reduced in human blood. Reduction leads to pronounced conformational changes within C4 that considerably affect the accessibility of the integrin-binding motif, and thereby impair integrin-mediated platelet binding. We also reveal that reduced species in the C4 domain undergo specific thiol/disulfide exchanges with the remaining disulfide bridges, in a process in which mechanical force may increase the proximity of specific reactant cysteines, further trapping C4 in a state of low integrin-binding propensity. We identify a multitude of redox states in all 6 VWF-C domains, suggesting disulfide bond reduction and swapping to be a general theme.

Conclusions: Our data suggests a mechanism in which disulfide bonds dynamically swap cysteine partners and control the interaction of VWF with integrin and potentially other partners, thereby critically influencing its hemostatic function.

KEYWORDS
biomechanical phenomena, blood platelets, disulfides, integrins, protein folding

1 | INTRODUCTION

The von Willebrand factor (VWF) is a large, mega-Dalton, multimeric, extracellular protein that is essential in achieving and regulating primary hemostasis [1]. Its mature monomers consist of 2050 amino acids, divided into 12 heavily disulfide-bonded protein domains (Figure 1A) [2,3]. It features 169 cysteines across its sequence [4], which are considered to be mainly paired in VWF multimers. They are associated with a variety of biological functions, most prominently the establishment of disulfide bridges between carboxy- and the amino-terminal domains assembling VWF monomeric units into dimers and multimers [1]. Other disulfide bonds protect the structural integrity of individual domains [1].

VWF is responsible for 2 essential hemostatic functions: adhesion of platelets to collagen at sites of vascular injury as well as the transportation and the half-life increase of factor (F)VIII through protective binding [1]. Mutations in the structure of VWF or dysregulation of its concentration in the bloodstream lead to severe, and often, life-threatening bleeding disorders. This medical condition, known as von Willebrand disease, exhibits a broad range of phenotypic responses ranging from acute hemorrhaging to thrombus formation [5]. Many of the known disease mutants are mutations of cysteines, highlighting their essential role in VWF function [6].

Triggered by the shear stress of flowing blood, VWF initiates the primary response to injury by recruiting platelets to the collagen matrix of the endothelium [7,8]. Under conditions of low hydrodynamic forces, VWF adopts a globular structure that gets elongated upon surpassing shear rates at the scale of $10^3 s^{-1}$ [8]. Here, the VWF A1 and A3 domains connect VWF to collagen [1] (Figure 1A) and the former binds to platelets via the interaction with the glycoprotein (GP)-Ibα receptor [7]. The tensile forces acting on the VWF multimer increase the binding affinity between A1 and GPIbα, independent of the shear rate and VWF elongation [9].

In contrast to these noncovalent force responses of VWF, the dynamics of the covalent binding states given by the disulfide connectivity, as a response to tensile forces from flowing blood, remain largely unknown. It is established that disulfide bonds drive VWF multimerization and protect it from unfolding under the influence of shear in the flowing blood [1]. Consequently, improper disulfide pairing is related to dimerization [10,11] and multimerization defects [12], as well as to the structural rearrangement and gain of function of the domain A1 [13]. Beyond conferring structural integrity, disulfide bonds have been recently discovered to directly participate in hemostatic functions. Thiol-disulfide shuffling has been suggested to mediate VWF multimer size [14], oligomerization [15,16], and platelet binding [17]. Moreover, the autoinhibition of VWF for the binding of platelets, initiated by A1–A2 interdomain interactions, is controlled by a disulfide bond switch in the VWF A2 domain [18]. In addition, blockage of free thiols in VWF has been reported to interfere with its binding to collagen [19]. Beyond VWF, other extracellular proteins involved in hemostasis are mechano-redox controlled. The shear-

Essentials

- Platelet integrins interact with the disulfide-bonded C4 domain of von Willebrand Factor (VWF).
- The redox state of disulfide bonds in C4 domain of VWF was studied by molecular simulations and experiments.
- Two bonds are reduced, causing C4 unfolding and disulfide swapping.
- Opening of disulfide bonds impairs integrin-mediated platelet binding.

dependent (de)adhesion of integrin αIIbβ3 to fibrinogen is an example of this [20]. Fibrinogen itself exists in a multitude of force-responsive covalent forms which dynamically exchange to drive fibrin polymerization [21].

Although the importance of cysteine redox states and disulfide connections has been recognized, structural data on the major disulfide bonded domains C and D have only very recently become available [2,16,22,23]. In particular, VWF contains 6 C-domains and the C-terminal cysteine-knot dimerization knot domain, which are rich in disulfide bonds (Figure 1A). Accordingly, a mechanistic and quantitative view on redox regulation as well as the role of force for such domains is currently lacking. We here focus on resolving the atomistic principles of disulfide bond reduction of the C4 domain of VWF. C4 plays a direct adhesive role as an anchoring point for platelets [24] and is the only C-domain, along with C6 [25] and the cystine-rich knot domain [26], whose structure has been experimentally determined (in the case of C4 by nuclear-magnetic resonance spectroscopy (NMR) [2]. C4 is a small 85-amino acid domain composed of 2 flexible subdomains, SD1 and SD2, and is structurally stabilized by 5 disulfide bridges (Figure 1B). It contains an integrin-binding RGD motif at the tip of the first β-hairpin in the SD1 subdomain, where it can connect to the platelet integrin receptor αIIbβ3 [1]. The C4 domain and, most importantly, the loop containing the RGD motif are topologically protected from mechanical unfolding by a set of disulfide bonds [2].

In this study, we asked if the redox states of inter-cysteine disulfide bonds in C4 dynamically regulate the presentation of RGD to platelets, which is one of the key functions of VWF. We addressed this question by integrating atomistic simulations with biochemical assays.

2 | METHODS

We determine the redox state of human VWF-C domain disulfides by liquid chromatography and mass spectrometry, from either human blood samples or recombinant VWF. To investigate the consequences of the C2570A and C2528A substitutions for VWF-C4's ability to bind
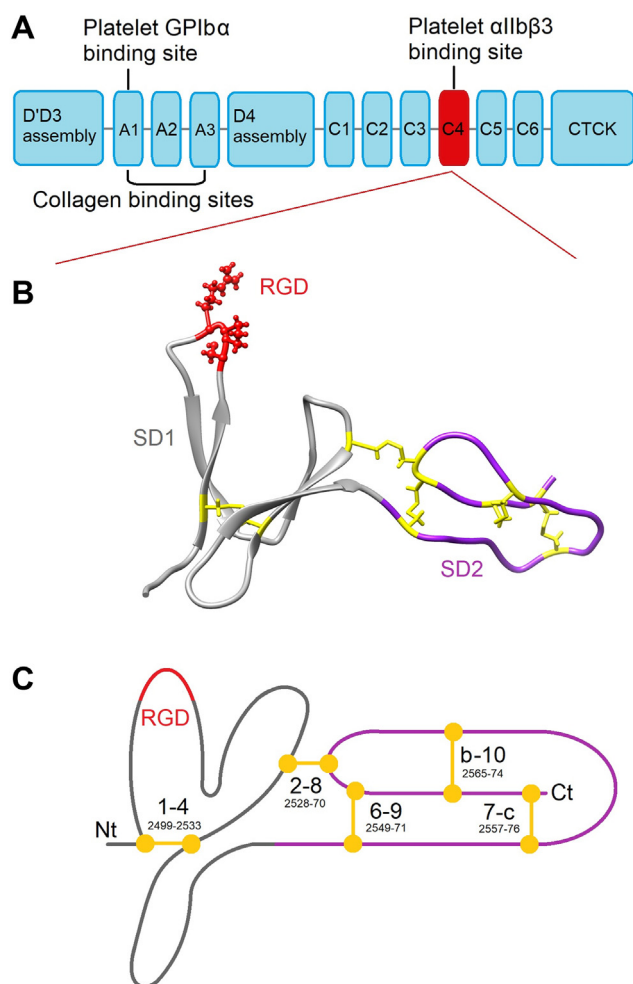
FIGURE 1 VWF-C4 domain: (A) Scheme of the VWF monomer, highlighting the position of the C4 domain. Platelet glycoprotein Ibα, integrin αIIbβ3, and collagen binding domains are indicated. (B) up: Cartoon representation of VWF-C4 (85 residues, 2493-2577 of the VWF sequence) according to its NMR structure [2]. The C4 integrin-binding motif (RGD, residues 2507-2509) and the 5 disulfide bonds are represented as sticks and spheres, the two subdomains (SD1 and SD2) are differentiated by color. (B) down: scheme of the VWF-C4 domain labeling the 5 disulfide bonds according to the overall VWF-C domain topology [3] (amino acids are also indicated).

platelet integrin, a platelet adhesion study was performed. Molecular dynamics (MD) simulations of the VWF-C4 domain were carried out, in its fully oxidized (FO) state and in 5 more situations with one of the disulfide bonds removed (1-4, 2-8, 6-9, 7-c, or b-10) (Figure 1). Simulations were performed under equilibrium conditions and applying force on the protein-termini, mimicking the elongational tension this domain would experience in the flowing blood (Figure 2). Additional quantum mechanics/molecular mechanics (QM/MM) simulations were carried out to study the disulfide bond exchange occurring upon the attack of the free sulfur 2 to the 1-4 bond, as this reaction can decide on the propensity of the RGD motif for binding to platelet integrins. See experimental and simulation details in the Supplementary Methods [27–59].

3 | RESULTS

3.1 | Tension-dependent conformations of the VWF-C4 domain with reduced disulfide bonds

C4 contains 10 cysteines, which have all been disulfide bonded in NMR structures [2] (Figure 1B). Fully oxidized, these bonds structurally stabilize C4, ensuring its ability to withstand the external shear force of the bloodstream (which in our simulations are represented by the external pulling forces acting on the termini of C4) and thereby guaranteeing its capacity to optimally bind to platelets via the interaction with integrin. Reduction of these bonds may alter the structural integrity of the C4 domain affecting integrin (and thus platelet) binding. Disulfide bond reduction would also leave free thiols as reaction products, opening up the possibility of disulfide exchange.

Hence, we first investigated the effect that the redox state of the disulfide bridges has on the conformation of the VWF-C4 domain under tension. We performed at least 10 force-probe MD simulations for each redox state (including the FO configuration) by pulling the termini of C4 away from each other, exerting different forces of ∼50, ∼100, and ∼500 pN (Figure 2). We monitored the separation between the termini as a function of time (Figure 2A).

As expected, the 5 (oxidized) disulfide bonds prevented the elongation of C4 upon the application of force. Only the termini were stretched, resulting in a maximum inter-termini separation of ∼7.9 nm (for a pulling force of 500 pN). Opening the disulfide bonds which are located solely within the SD2 subdomain, namely, 6-9, 7-c, or b-10, resulted in similar elongation lengths as for the FO protein. This is reflected in similar conformations for the FO, 6-9, 7-c, and b-10 cases (the ribbon structure snapshots are shown in Figure 2B).

In contrast to this, we observe major unfolding in all 10 individual simulations if bond 1-4 is reduced and a force of 500 pN is applied. At lower forces and within the simulation time scale of ∼100 ns, only intermediate elongations of ∼12.9 nm were observed upon reduction of the 1-4 bond (8 cases at 100 pN and 1 case at ∼50 pN out of n = 10 simulations for each force). The geometry of the unfolding process is depicted in Figure 2B, cases 1-4a (full unfolding) and 1-4b (partial unfolding, β-hairpin structure near sulfur 4 still completely intact). Here, the application of force led to a complete flattening of the β-hairpin containing the RGD motif upon unfolding for all forces but only for 500 pN we also see a dismantling of the double β-hairpin structure present in SD1 into a single β-hairpin, namely the one carrying the bond 2-8 (state 1-4b in Figure 2). The final unfolding length in this case is ∼15.9 nm for the entirety of C4.

For 2-8, at a lower force regime, only a residual stretching of the termini was observed, with an elongation similar to the FO case (state 2-8b in Figure 2). The strength of the β-strand within SD1, formed between sulfur 4 and 6, was sufficient to protect the structure from unfolding even in the absence of disulfide bond 2-8. The simulation time scale (∼100 ns) limited the observation of full force-induced opening conformational transitions for 50 pN and 100 pN. To overcome this issue, we applied a high force of 500 pN. In this case, reduction of bond 2-8, which connects SD1 and SD2 triggered a major
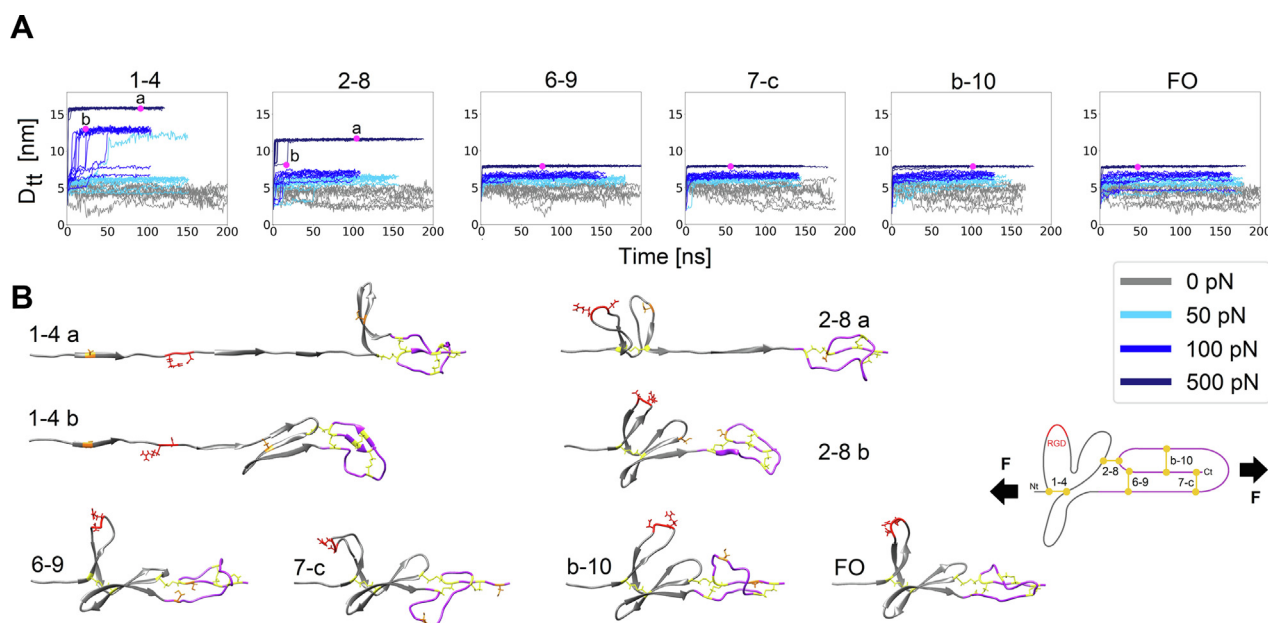
FIGURE 2 Tension-induced elongation of the VWF-C4 domain upon disulfide bond reduction. A: Elongation of the C4 domain under force was measured by the distance between termini (Dtt), in the fully oxidized case (FO) and after reducing the indicated disulfide bond upon application of a constant force F (different force values depicted with a different color). B: Examples of structures at the instants indicated with the magenta dots in A are displayed (SD1 region: gray; SD2 region: purple; RGD motif: red; closed disulfide bonds: yellow, reduced disulfides: orange). At the right, a scheme of the protein highlighting the disulfide bonds is included.

unfolding event, resulting in final elongations of ∼11.5 nm (Figure 2B, 2-8a).

Note that in our simulations, we tested the effect of reduction of either disulfide bond, separately. From our data, it is reasonable to assume that if both 1-4 and 2-8 bonds are reduced at the same time, their unfolding effect adds up causing a complete flattening of the entire SD1 subdomain. All observed elongations are comparable to previously reported values [19]. Thus, force impacts the secondary and tertiary structure of the C4 domain, provided that either disulfide bond 1-4 or 2-8 is reduced.

3.2 | C4 disulfide bonds 1-4 and 2-8 are partially reduced

The reduction of the 1-4 and 2-8 bonds induced large unfolding of C4. In addition, cysteines 1, 4, 2, and 8 have already been observed as free thiols in C4 [17]. Thus, we asked for VWF-C4 in human blood if the 1-4 and 2-8 bonds could partially exist in a reduced state and if that is the case whether the reduction of these could cause meaningful alterations in C4's function. Accordingly, we investigated the redox state of C4's disulfide bonds in the plasma of 10 healthy human donors *ex vivo*, using mass spectrometry (Figure 3A). Although the 2 bonds were predominantly oxidized, a small fraction of the 1-4 and 2-8 bonds was on average 3.4% and 2.7% reduced in the population of the VWF molecules, respectively. This result indicates that the C4 domain disulfide bonds 1-4 and 2-8 indeed have the potential to be labile. We were not able to detect reduced peptides for the other 3

disulfide bonds, but cannot fully exclude their presence in human blood. Taken together, we have experimental evidence for 2 partially reduced disulfide bonds in C4, 1-4, and 2-8, which is consistent with previous research [17].

Note that it is very likely that among the approximately 10^{12} molecules of healthy human donor VWF, both disulfide bonds are reduced in some molecules, one or the other bond is reduced in other molecules, and both are oxidized in some molecules, although our analysis is unable to determine the oxidation state of individual molecules.

In addition, we have measured the redox state of the Cys2499-Cys2533 and Cys2528-Cys2570 disulfide bonds in the plasma of 5 patients with heart failure receiving extracorporeal membrane oxygenation support and in patients not receiving this mechanical assistance (see Table S2). The redox states of the bonds were within the same range in both patient groups, indicating that this external stimulus does not appreciably change the states of these C4 disulfide bonds.

3.3 | Genetic ablation of either 1-4 or 2-8 bond impairs platelet immobilization

In blood, the strained 1-4 and 2-8 bonds also exist in a reduced state (Figure 3A) and C4 undergoes pronounced unfolding transitions under such conditions (Figure 2). These 2 observations led us to ask if the C4-disulfide lability has functional consequences. To this end, we examined the effect of ablating these bonds on platelet adhesion.
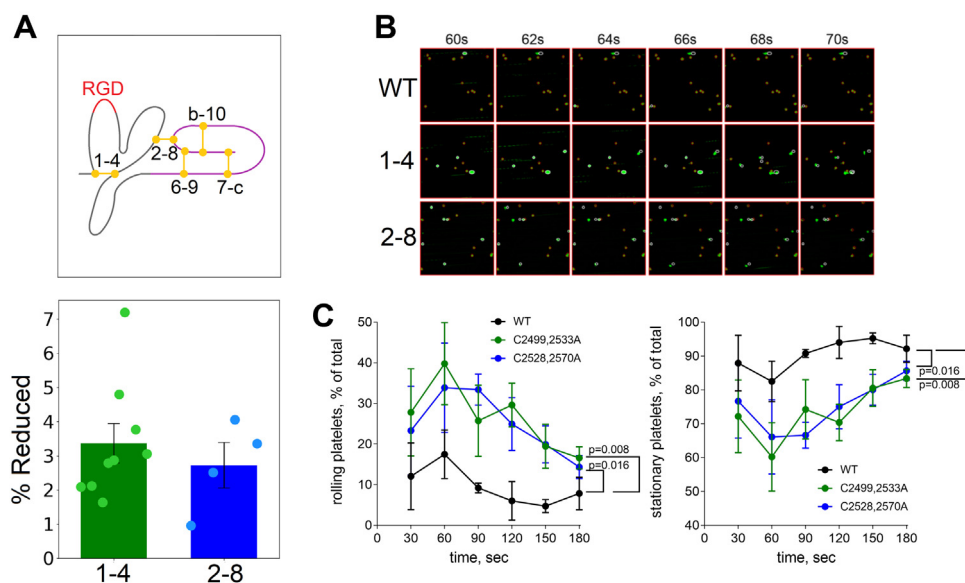
FIGURE 3 Disulfide bonds 1-4 and 2-8 in the VWF-C4 domain are partially reduced in blood and their genetic ablation impairs engagement of the C4 RGD motif with platelet integrin under fluid shear conditions. A: Reduction state of C4 disulfide bridges in healthy human donors. Shown is the percentage of reduced bonds for each patient (dots), the mean value of all patients (green and blue bars) as well as the standard deviation on the mean (black error bars). See above the scheme of the C4 indicating the location of these 2 bonds. B: Washed human platelets were perfused over VWF matrices at a shear rate of 1000 s^{-1} for 3 minutes. Examples of rolling and stationary platelets between 60 seconds and 70 seconds of perfusion are shown for the wild-type protein and the variants with either the 1-4 or the 2-8 removed by alanine substitution of the cysteines. C: Percentage of rolling and stationary platelets as a function of time of perfusion is displayed (mean ± SEM of 4 biological replicates). All p-values were assessed by 1-way Kruskal–Wallis test with Dunnett's multiple comparisons post-hoc compared with wild-type.

Accordingly, the 1-4 or 2-8 disulfides were eliminated by mutating both cysteines of the bond to alanines. The wild-type and mutant proteins were expressed in human embryonic kidney cells and collected from conditioned medium. The redox states of the C4 domain disulfides of the recombinant proteins were measured to ensure that elimination of either one of the C4 bonds did not change the redox state of the other one or other C-domain bonds in general. The disulfide status of recombinant wild-type and C4 domain disulfide mutants was very similar (Supplementary Figure S2). Moreover, the redox state of the recombinant proteins was comparable to human plasma VWF (Figures 3A and 7 and Supplementary Figure S2). Thus, mutations did not alter the redox state of other C-domains.

Washed resting human platelets were perfused over VWF matrices at a shear rate of 1000 s^{-1} and the number of stationary and rolling platelets was measured at 30-second intervals (Figure 3B). Elimination of either the 1-4 or 2-8 VWF-C4 disulfide bond resulted in significantly more rolling and fewer stationary platelets (Figure 3C). Therefore, the 1-4 and 2-8 VWF-C4 disulfide bonds need to be intact for efficient engagement of the C4 RGD motif with platelet αIIbβ3 integrin.

Note that addition of the blocking anti-αIIbβ3 monoclonal antibody Reopro (n = 1) resulted in an increased number of rolling platelets on wild-type VWF but no change in the VWF disulfide mutants (Supplementary Figure S3). This data supports our conclusion that the impaired engagement of αIIbβ3 with the C4 RGD motif is due to the C4 disulfide mutations independent of the GP1bα-VWF A1 interaction.

Our MD simulations provided a molecular explanation for this reduction in platelet binding affinity. Without the stabilizing 1-4 bond, application of an external force, mimicking the elongational tension C4experiences due to the shear of the flowing blood [1,60], increased the probability of flattening the β-hairpin containing the integrin-binding RGD motif (see the non-zero probability for the angle $\theta \sim$ 180° when the force was not 0 in Figure 4A, left). From a geometric standpoint, this conformation is not likely to be optimal for binding as indicated by the β-hairpin opening angle and Ramachandran plot for the 3 amino acids of the RGD motif. In addition, we compared the RGD motif backbone torsion angles observed in the simulations (after full expansion) with those measured in X-ray structures of RGD-containing ligands bound to integrins. The angles observed in the X-ray structures are close to those sampled in the force-free simulations, but this situation changes upon application of force. Especially, the ARG and ASP angles calculated in the simulations are increasingly distributed far from the experimental references as the pulling force increases. Considerable deformation of the RGD motif thus undermines optimal binding of integrin (and thereby of platelets) to the VWF mutant lacking the 1-4 bond.

The same argument cannot be applied to the mutant with bond 2-8 eliminated. Reducing this bond displayed no major effect on the conformation of the RGD binding β-hairpin (Figure 4B). In this case,
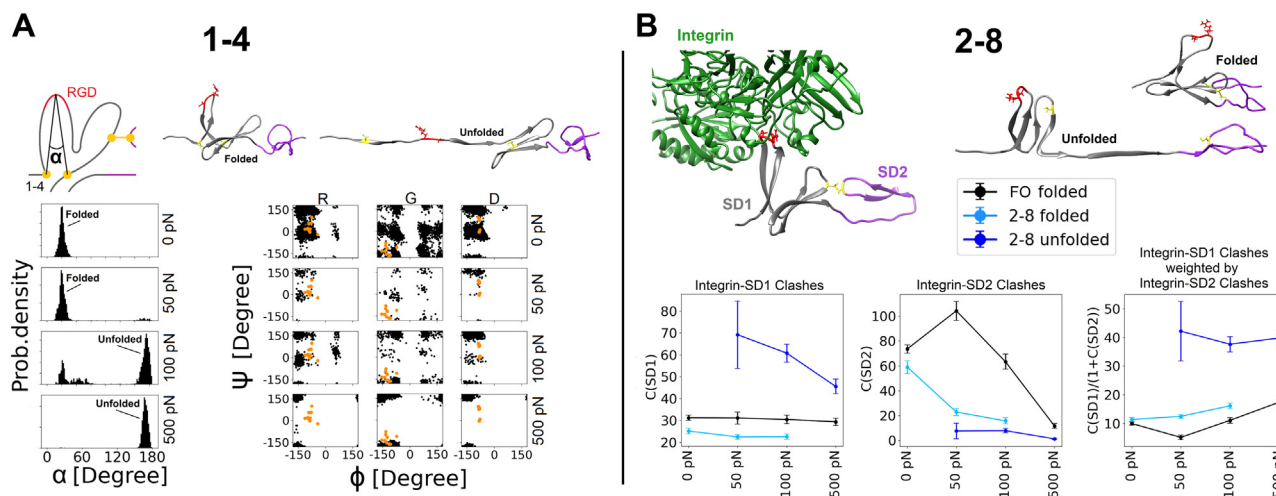
FIGURE 4 Alteration and accessibility of the RGD motif under force reduce binding to integrin of 1-4 and 2-8 reduced VWF-C4 variants. A: Bond 1-4 is reduced. RGD β-hairpin angle formed by Cys2499 (1), Gly2508 (G) of the RGD domain, and Cys2533 (4) (see scheme) (left panels), as well as Ramachandran angles ⍴ and ψ for the RGD motif (right panels), were recovered from simulations with the bond 1-4 reduced, under different forces (see labels at different horizontal panels). Cartoons at the top exemplify the folded ($\alpha \sim 30°$) and unfolded ($\alpha \sim 180°$) conformations of the RGD-containing β-hairpin (SD1: gray; SD2: purple; RDG motif: red, and cysteines: yellow). 13 orange dots in the Ramachandran plots represent angles taken from X-ray structures of RGD peptides in complex with integrin [74]. B: The model of the complex formed by VWF-C4 (grey and purple) and αIIbβ3 integrin (green) was predicted by the alphafold (top-left cartoon). Right of it, snapshots of C4 with the 2-8 bond reduced in folded and unfolded configurations are presented. The three panels below show the average number of clashes, C, of the heavy atoms of the C4 subdomains with the backbone atoms of integrin. C was calculated separately for SD1 (left panel) and SD2 (middle panel) and shown as a function of the applied force. The clashes of subdomain SD1 were also weighted by those of SD2 according to C(SD1)/(1 + C(SD2)) and subsequently averaged (right panel). Colors differentiate the three considered oxidation states of the 2-8 bond along with the conformation of C4. FO folded = fully oxidized C4 domain in the folded state, 2-8 folded = C4 domain with bond 2-8 reduced, before unfolding has taken place, 2-8 unfolded = C4 domain with bond 2-8 reduced, after unfolding has taken place. In all cases, time averages ± SEM are presented.

the existent 1-4 bond is sufficient to stabilize the RGD β-hairpin. However, as soon as the connection between the second β-hairpin of SD1 (carrier of cysteine 2) and the subdomain SD2 is broken, an increased propensity to occlude the RGD binding β-hairpin is observed, as explained in the following. We predicted the conformation of the complex formed by αIIbβ3 integrin and the VWF-C4 domain using alphafold [46,47] (Figure 4B, top-left cartoon). Note that alphafold's sole input is the primary structure of both proteins, ie, no further structural data were provided. Separately, the predicted structures of C4 and integrin were almost identical to the experimentally-determined ones, with a root mean square deviation of 0.45 nm for C4 (compared with the NMR structure [2] with PDB ID 6FWN) and 0.09–0.40 nm for integrin (compared with the X-ray structure [61] with PDB ID 3T3P, 0.09 nm for chain A and 0.4 nm for chain B). Thereafter, we fitted randomly selected conformations of C4 to the predicted alphafold structure, by overlaying the RGD β-hairpin. We carried out this fitting procedure, separately for conformations of C4 in its FO state, or with the 2-8 bond reduced, either in folded or unfolded configurations (Figure 4B, top-right cartoons) (see detailed explanation of the fitting procedure in the Supplementary Methods).

Upon reduction of 2-8, the second beta-hairpin of SD1, which carries sulfur 2, gets into close contact with the RGD β-hairpin, an effect that would not occur if the second β-hairpin was still connected to SD2 by the 2-8 bond (Figure 4B, top-right cartoons). We investigated the effect this may have for the interaction of C4 with integrin

by measuring clashes between the backbone atoms of integrin and the heavy atoms of the VWF-C4 SD1 subdomain. The reduction of the 2-8 bond and subsequent unfolding under force increased the number of clashes compared with the case of an FO and folded C4 as well as for a C4 domain with reduced 2-8 bond that is still folded (Figure 4B, bottom left panel). The predicted number of clashes between the SD2 subdomain and integrin displayed the opposite trend, ie, less clashes were observed when 2-8 was reduced (Figure 4B, bottom middle panel). In nature, these SD2 clashes could easily be alleviated upon binding by the large hinge-flexibility of the C4 domain [2]. But this flexibility cannot be incorporated in our docking and fitting procedure, so a high number of SD2 clashes just indicates a fit of lower quality. Accordingly, to correct for this limitation, the clashes of SD1 were weighted by those of SD2, assigning a higher weight to conformations in which the number of clashes of SD2 was low (Figure 4B, bottom right panel). Reassuringly, this weighting did not modify the original trend regarding the number of clashes between SD1 and integrin upon reduction of the 2-8 bond. From this analysis, we suggest 2-8 reduction hampers integrin–VWF C4 binding by steric hindrance.

3.4 | C4 undergoes disulfide bond shuffling

The reduction of either the 1-4 or 2-8 disulfide bonds results in the free thiols, which by getting into proximity could attack still-formed
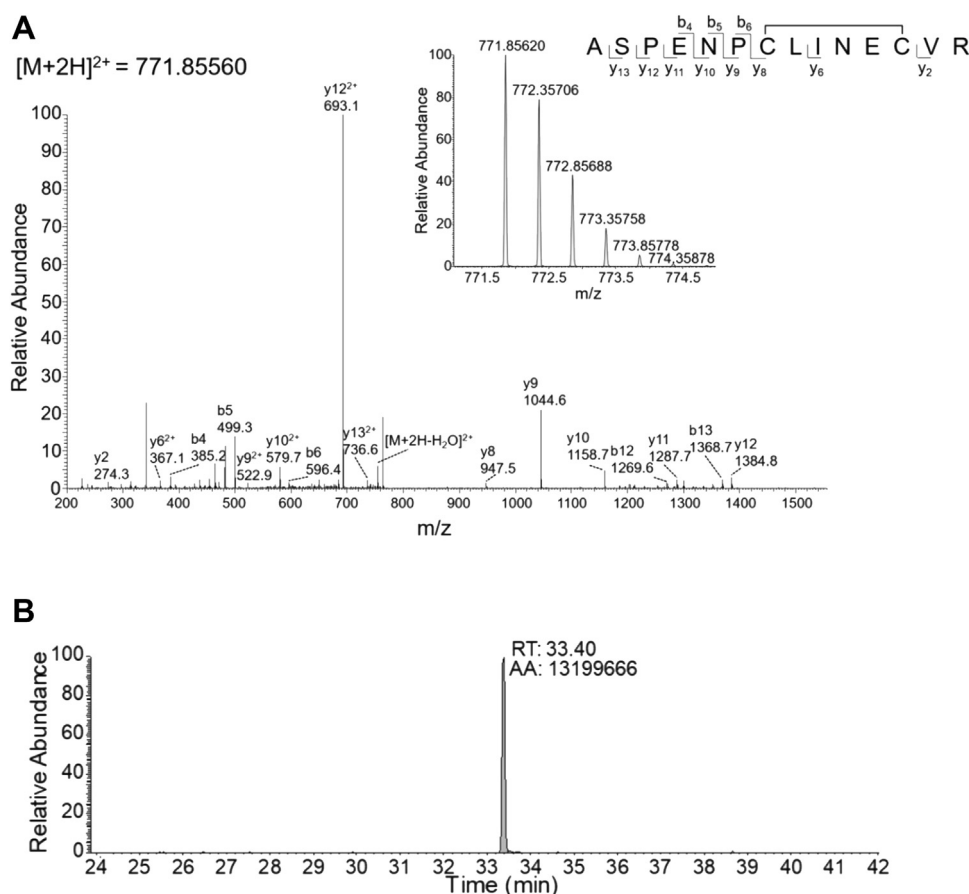
FIGURE 5 VWF-C4 undergoes disulfide bond shuffling: (A) Representative tandem mass spectra of the ASPENPCLINECVR peptide. The accurate mass spectrum of the peptide is shown in the inset (observed $[M + 2H]^{2+}$ = 771.85620 m/z and expected $[M + 2H]^{2+}$ = 771.85560 m/z). (B) High performance liquid chromatography resolution of the C4 domain ASPENPCLINECVR peptide containing the C2528-C2533 (2-4) disulfide bond (cysteines underlined at the peptide sequence).

disulfide bonds. We tested this hypothesis *ex vivo*. VWF was immunoprecipitated from healthy donor plasma, digested with chymotrypsin and trypsin, peptides resolved by high performance liquid chromatography, and analyzed by mass spectrometry (see methods for details). The C4 domain ASPENPCLINECVR peptide containing the Cys2528-Cys2533 (2-4) disulfide bond was identified with very high confidence (p = 0.00066) (Figure 5). In addition to this new bond formed inside C4, the free cysteine 1 (C2499) established a bond with the cysteine C2494 (C3-10) of the neighbor C3 domain, as reflected by identification of the CLPSACEVVTGSPR peptide (Supplementary Figure S5). Consequently, disulfide bonds undergo intra-C4 and C3-C4 interdomain disulfide bond swapping.

We investigated the molecular origin of the experimentally observed preferential swap. Proximity between free thiols has been suggested to be a key factor for disulfide bond swapping [62]. We tested if, under the application of force, the inter-sulfur distances in SD1 changed after the reduction of 1-4 or 2-8 bond. We found that indeed, for the resulting 4 cases, inter-sulfur distances shifted considerably toward lower distance values upon force application of a force of 500 pN (Figure 6A). The same general effect could not be observed with low forces, presumably owing to insufficient sampling.

However, still attacking sulfur 2 maintained the tendency to occupy a lower distance at a low force of 50 pN or 100 pN in an extra set of simulations starting from a fully-elongated configuration. Consequently, force, by bringing the free thiol 2 into closer proximity to the attacked disulfide bond 1-4 appears to be an important factor defining one of the observed disulfide exchange reactions.

The proximity argument from MD simulations underlined the important role force plays in bringing free thiols into close proximity. However, it did not resolve between the specific thiol being attacked. In particular, the free thiol 2 approached with similar probability both cysteines 1 and 4, while in mass spectrometry only binding to cysteine 4 could be verified (Figure 5). To compare the involved free energy changes of these swaps, we carried out QM/MM simulations using metadynamics and density-functional tight binding for the QM region. We concentrated on the attack of sulfur 2 on the 1-4 bond (Figure 6B), as this reaction can decide on the propensity of the RGD motif for binding to platelet integrins (see Figure 6B-C). Figures 6B and C depict the two-dimensional projection of the free energy surface and a simplified energy scheme, respectively, determined from a series of exchange reactions between sulfur 1, 2, and 4. While the transition barriers are equally high for both exchange options, the local minimum of configuration 2-4 lies
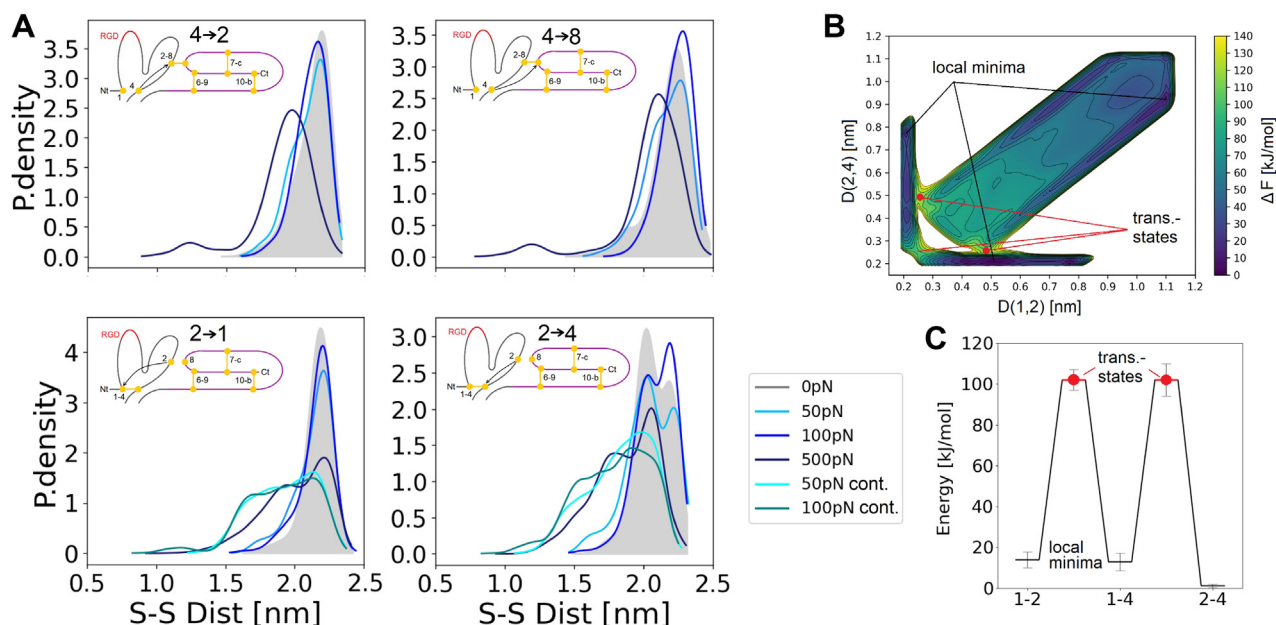
FIGURE 6 Force-mediated proximity along with thermodynamic affinity explains specific disulfide bond shuffling in VWF-C4. (A) Inter-sulfur distance probability distributions when either cysteine 4 or cysteine 2 is unpaired. Distance is presented for the indicated 4 sulfurs that could pair, under equilibrium (gray) and forced (blue shades) conditions. See all inter-cysteine distances in Supplementary Figure S4. A schematic representation of the possible thiol-disulfide exchange pathways is indicated at the inset. (B) Free energy surface for the attack of the 2 free thiols to the 1-4 bond determined from quantum mechanics/molecular mechanics calculations (situation depicted at the bottom panels in A). The x- and y-axes represent the inter-sulfur distance. Here, an external force of 166 pN was applied to the C4 termini. (C) Energy minima and transition barriers extracted from (B), the black line marks the average result of all meta dynamics simulations. Error bars represent SEM. Transition states are indicated with red dots. The energy minimum of 2-4 is significantly lower than those of 1-2 and 1-4, $p < .02$.

significantly lower than those of all other permutations, a result that aligns very well with the experimental findings and that suggests 2-4 to be thermodynamically preferred over 1-2.

3.5 | Beyond C4: All VWF-C domains are partially reduced

Motivated by the analysis of C4, we finally studied the prevalence of reduced disulfide bonds in the entire VWF-C domain family.

Accordingly, the redox state of 17 disulfide bonds in the 6 C-domains was quantified (Figure 7). All 17 bonds were predominantly oxidized in 10 healthy human donors (Figure 7). A small fraction of these bonds, however, were on average 1%–5% reduced in the population of the VWF molecules. Interestingly, the observed frequency of bond reduction increases from C1 to C6 with greater proximity to the cysteine-rich knot of the VWF. The 7-10 bond in C5 and C6 show the highest fraction of reduced VWF molecules, namely 6.5% and 7.3%, respectively. Consequently, not only C4 but all VWF-C domains have the potential to be labile.
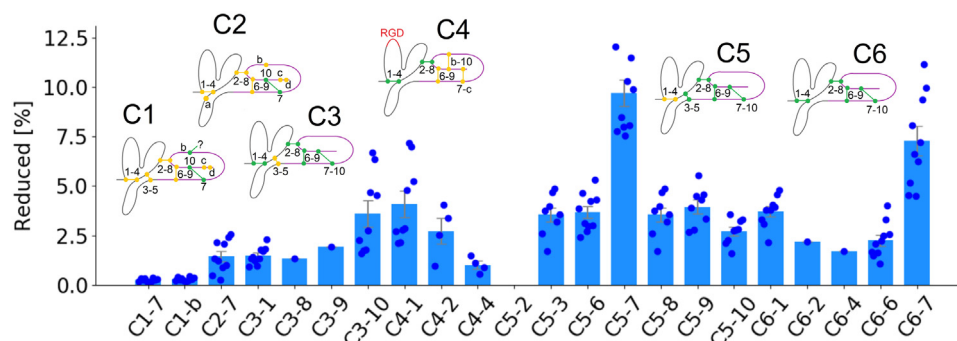
FIGURE 7 Redox states of 17 VWF-C domain disulfides in 10 healthy human donors (5 males and 5 females, aged 22-58 years old). The 17 bonds that have been analyzed for redox state are colored in green. Blue dots are experimentally measured in individual donor blood. The bars and errors are mean ± S.E.M.

4 | DISCUSSION

In this study, we investigated the structural and functional consequences of disulfide bond breakage and exchange for the VWF-C4 domain by molecular simulations; mass spectrometry; and platelet binding assays, in equilibrium and under force. We started our analysis with the observation that an FO C4 domain is crosslinked by disulfides to an extent that locks the domain in a folded force-unresponsive state (Figure 2). Partial reduction of specific bonds, however, enabled large conformational changes, thiol/disulfide exchange reactions, and mechano-redox regulations of integrin binding.

Two of the 5 disulfide bonds present in C4, namely, 1-4 and 2-8, both located at the SD1 sub-region (Figure 1) displayed a distinct behavior. Previous mass spectroscopy experiments [17] as well as our experiments showed these 2 bonds to be reduced in the blood (Figure 3A). Their process of reduction itself is possibly catalyzed by a reducing agent, such as glutathione, or a redox enzyme, such as protein-disulfide isomerase [11]. In addition, we find these 2 bonds to play a critical role in the structural integrity of the C4 domain, as their reduction leads to force-mediated distortions in the secondary and tertiary structures of the C4 domain (Figure 2). Hence, our combined findings provide evidence for the existence of at least 2 reduced redox states within the VWF-C4 domain and point toward a dramatic conformational alterations of this domain by the action of mechanical forces, such as those originating from the shear of the flowing blood, upon reduction.

The main biological function of the C4 domain is the reinforcement of platelet binding by the interaction of its RGD motif with the platelet integrin receptor αIIbβ3. Platelet binding assays revealed a decrease in integrin-binding capacity for VWFs where either the 1-4 or 2-8 bond was erased through mutation (Figure 3B, C). Our MD simulations link this reduction in binding ability (compared with the wild-type VWF) to a force-enhanced flattening (1-4) or steric occlusion (2-8) of the RGD β-hairpin (Figure 4). Thus, our data show that reduction of these 2 specific disulfide bonds does not merely destabilize the C4 domain, but more importantly, compromises its main function of anchoring platelets to VWF in a force-dependent manner. It is important to note that we cannot exclude other redox states of C4, involving the other disulfide bridges. Our mass spectrometry analysis allowed the detection of only 2 of 5 bonds in their reduced state, and we followed up on these 2 in our subsequent mutagenesis study. Our MD simulations highlight the role of 1-4 and 2-8 bonds in keeping the C4 topology intact, and thus hint at their extraordinary role in regulating C4 function, but a similar role cannot be excluded for the other C4 bonds.

The GP1bα–VWF A1 interaction is characterized by a fast dissociation rate that cannot support irreversible platelet adhesion. Platelets tethered only via this interaction rolling constantly in the direction of the fluid flow. This transient interaction allows the establishment of additional bonds primarily with αIIbβ3 integrin via the VWF C4 RGD motif that results in transition from rolling to stable platelet adhesion [24]. We could not measure the speed of the rolling platelets in our system, although this is expected to be governed by the GP1bα-VWF A1 interaction. These interactions predominantly occur with VWF tethered to endothelium or exposed collagen, which is an extended configuration that exposes the binding sites. In addition, the soluble globular VWF is not expected to bind circulating platelets due to masking of binding sites. Moreover, because resting platelets were used for all microfluidic flow assays, the platelet interaction with the wild-type C4 domain does not require fully active αIIbβ3 integrin. We cannot rule out, however, that some platelet activation occurred because of the mechanical stresses associated with platelet preparation. The current evidence is that αIIbβ3 integrin adopts a range of configurations between fully closed and fully open that has a corresponding range of affinities for fibrinogen, and likely also for VWF [63]. Whether VWF binds to αIIbβ3 in a resting or active conformation, therefore, probably does not have a binary answer.

Blockage of free thiols has been reported to interfere with the binding of VWF to collagen [19] and to platelets [17]. Moreover, the methionine oxidation of VWF can regulate the protein's force response and vice versa [64,65]. Furthermore, autoinhibition of the VWF for the initial binding of platelets is controlled by a disulfide bond in the VWF A2 domain [18]. Our study identifies the key molecular transitions in C4 that alter VWF-integrin binding. It thereby provides a structural and dynamic molecular explanation of how mechanical and redox stimuli jointly control VWF function. We propose that high levels of oxidative stress, eg, in the form of reactive oxygen species, decrease stable integrin-mediated platelet binding, whereas high amounts of shear forces in blood push VWF into a less adhesive state under high oxidative stress conditions. In this scenario, processes with elevated oxidative stress levels, such as inflammation or immune response, could corroborate thrombotic disorders. Such mechano-redox crosstalk is emerging as a common theme also for other extracellular proteins such as integrins [20] or fibrinogen [21].

Disulfide bond reduction leads to the introduction of free thiols that could promote disulfide bond exchange. In fact, our mass spectrometry findings demonstrate the formation of a new intra-C4 bond, between the cysteines 2 and 4 (Figure 5), as well as across domains C3 and C4, between cysteine 10 of C3 and cysteine 1 of C4 (Supplementary Figure S5). Interestingly, disulfide bond swapping in the C2 domain is involved in VWF oligomerization [15]. It would be highly interesting to test if intermolecular disulfide swapping across C3 and C4 domains occurs between different VWF multimers. It would thereby promote VWF network formation and in this way complement non-covalent VWF assembly under shear conditions [66]. It has been recently shown that the VWF A1 domain still can bind to GP1bα even in the absence of its constraining disulfide bond [13,67]. However, C4 and A1 have very different structural folds. In particular, in C4, the Cys2499-Cys2533 bond directly protects the integrin RGD binding site, whereas, in A1, the disulfide bond constrains the whole domain. We thus think that the mechanism by which disulfide bond reduction alters the interaction of these domains with the platelet receptors is different.

The mechanochemistry of disulfides has been intensively studied [68,69]. Intramolecular thiol/disulfide exchange, catalyzed by mechanical force, has remained difficult to be observed in biological

systems. Instead, disulfide bond swapping is considered to require enzymatic catalysis eg, by PDI [11,70]. To our knowledge, direct observation of a non-enzymatic exchange has so far only been possible for an immunoglobulin domain engineered for this purpose [68]. Here, we show that the reduction of VWF in a stretched conformation brings specific thiols (thiol 2) close enough to one of the exchange candidates (1-4) so that swapping can occur (Figure 6A). Proximity between the free sulfur and the attacked bond has indeed been suggested to be a key factor mediating disulfide-bond exchange [62,71–73]. Also, from an energetic point of view, the attack of the free thiol 2 on either bonded sulfur 1 or 4 is similarly likely, although a slightly increased preference for 2-4 was observed (Figures 6B–C). The formation of the experimentally validated 2-4 bond would leave the RGD binding β-hairpin unprotected and prone to unfolding under the influence of external force, akin to the situation we observed when 1-4 was reduced (Figure 4A). Thus, reduced integrin (and therefore platelet) binding of C4 due to complete flattening of the RGD binding site of VWF could also be a result of 2-8 to 2-4 disulfide bond exchange.

Resting platelets were used in all microfluidic flow assays. Our data imply that platelet interaction with the C4 domain does not require fully active αIIbβ3 integrin. We cannot rule out, however, that some platelet activation occurred as a result of mechanical stresses during platelet preparation. The current evidence is that αIIbβ3 integrin adopts a range of configurations between fully closed and fully open that have a range of affinities for fibrinogen, and likely also for VWF [74]. Whether VWF binds to αIIbβ3 in a resting or active conformation, therefore, probably does not have a binary answer.

Our mass spectrometry data confirm the widespread occurrence of partially reduced disulfide bonds across all 6 C-domains (Figure 7). Interestingly, the extent of reduction of disulfide bonds overall increased from the C1 to the C6 domain close to the C-terminal cysteine-knot. Homologous to C4, the C3, C5, and C6 domains exhibit partially reduced 1-4 bonds, suggesting pronounced force-induced unfolding of the N-terminal loop of these domains, with potential implications of stem formation [75].

In summary, we here establish the molecular determinants governing dynamic changes in the topology of VWF-C4's disulfide bonds and the functional consequences of these changes on integrin-mediated platelet binding. Beyond structural integrity, mechano-sensitive disulfide bond redox control emerges as a prominent mechanism for the regulation of VWF function.

AUTHOR CONTRIBUTION

F.K. performed and analyzed the MD simulations and wrote the main part of the manuscript. D.B. performed and analyzed the experiments and wrote the corresponding parts of the manuscript. A.L. performed and analyzed the experiments. D.M. performed and analyzed the QM/MM calculations and wrote the corresponding parts of the method section. J.C. performed and analyzed the experiments. H.W. performed and analyzed the experiments. T.K. analyzed the QM/MM calculations and assisted in writing the manuscript. M.E. supervised the QM/MM calculations and writing of the manuscript. C.A.-S. analyzed the MD simulations and assisted in writing the manuscript. P.H. supervised the experiments and writing of the manuscript. F.G. supervised the MD simulations and writing of the manuscript.

DECLARATION OF COMPETING INTERESTS

We report that there are no conflicts of interest.

REFERENCES

[1] Springer TA. Von Willebrand factor, Jedi knight of the bloodstream. *Blood*. 2014;124:1412–25.

[2] Xu ER, von Bülow S, Chen PC, Lenting PJ, Kolšek K, Aponte-Santamaría C, Simon B, Foot J, Obser T, Schneppenheim R, Gräter F, Denis CV, Wilmanns M, Hennig J. Structure and dynamics of the platelet integrin-binding C4 domain of von Willebrand factor. *Blood*. 2019;133:366–76.

[3] Zhou YF, Eng ET, Zhu J, Lu C, Walz T, Springer TA. Sequence and structure relationships within von Willebrand factor. *Blood*. 2012;120:449–58.

[4] Titani K, Kumar S, Takio K, Ericsson LH, Wade RD, Ashida K, Walsh KA, Chopek MW, Sadler JE, Fujikawa K. Amino acid sequence of human von Willebrand factor. *Biochemistry*. 1986;25:3171–84.

[5] Schneppenheim R, Budde U. Von Willebrand factor: the complex molecular genetics of a multidomain and multifunctional protein. *J Thromb Haemost*. 2011;9(Suppl 1):209–15.

[6] van Schooten CJ, Tjernberg P, Westein E, Terraube V, Castaman G, Van Mourik JA, Hollestelle MJ, Vos HL, Bertina RM, van den Berg HM, Eikenboom JCJ, Lenting PJ, Denis CV. Cysteine-mutations in von Willebrand factor associated with increased clearance. *J Thromb Haemost*. 2005;3:2228–37.

[7] Bryckaert M, Rosa JP, Denis CV, Lenting PJ. Of von Willebrand factor and platelets. *Cell Mol Life Sci*. 2015;72:307–26.

[8] Schneider SW, Nuschele S, Wixforth A, Gorzelanny C, Alexander-Katz A, Netz RR, Schneider MF. Shear induced unfolding triggers adhesion of von Willebrand factor fibers. *Proc Natl Acad Sci U S A*. 2007;104:7899–903.

[9] Fu H, Jiang Y, Yang D, Scheiflinger F, Wong WP, Springer TA. Flow-induced elongation of von Willebrand factor precedes tension-dependent activation. *Nat Commun*. 2017;8:324.

[10] Brehm MA, Huck V, Aponte-Santamaría C, Obser T, Grässle S, Oyen F, et al. Willebrand disease type 2A phenotypes IIC, IID and IIE: a day in the life of shear-stressed mutant von Willebrand factor. *Thromb Haemost*. 2014;112:96–108.

[11] Lippok S, Kolšek K, Löf A, Eggert D, Vanderlinden W, Müller JP, König G, Obser T, Röhrs K, Schneppenheim S, Budde U, Baldauf C, Aponte-Santamaría C, Gräter F, Schneppenheim R, Rädler JO, Brehm MA. Von Willebrand factor is dimerized by protein disulfide isomerase. *Blood*. 2016;127:1183–91.

[12] Tjernberg P, Vos HL, Castaman G, Bertina RM, Eikenboom JCJ. Dimerization and multimerization defects of von Willebrand factor due to mutated cysteine residues. *J Thromb Haemost*. 2004;2:257–65.

[13] Tischer A, Machha VR, Frontroth JP, Brehm MA, Obser T, Schneppenheim R, Mayne L, Walter Englander S, Auton M. Enhanced local disorder in a clinically elusive von Willebrand factor provokes high-affinity platelet clumping. *J Mol Biol*. 2017;429:2161–77.

[14] Ganderton T, Berndt MC, Chesterman CN, Hogg PJ. Hypothesis for control of von Willebrand factor multimer size by intra-molecular thiol-disulphide exchange. *J Thromb Haemost*. 2007;5:204–6.

[15] Ganderton T, Wong JWH, Schroeder C, Hogg PJ. Lateral self-association of VWF involves the Cys2431-Cys2453 disulfide/dithiol in the C2 domain. *Blood*. 2011;118:5312–8.

[16] Anderson JR, Li J, Springer TA, Brown A. Structures of VWF tubules before and after concatemerization reveal a mechanism of disulfide bond exchange. *Blood*. 2022;140:1419–30.

[17] Choi H, Aboulfatova K, Pownall HJ, Cook R, Dong JF. Shear-induced disulfide bond formation regulates adhesion activity of von Willebrand factor. *J Biol Chem*. 2007;282:35604–11.

[18] Butera D, Passam F, Ju L, Cook KM, Woon H, Aponte-Santamaría C, Gardiner E, Davis AK, Murphy DA, Bronowska A, Luken BM, Baldauf C, Jackson S, Andrews R, Gräter F, Hogg PJ. Autoregulation of von Willebrand factor function by a disulfide bond switch. *Sci Adv*. 2018;4:eaaq1477.

[19] O'Brien HER, Zhang XF, Sanz-Hernandez M, Chion A, Shapiro S, Mobayen G, Xu Y, De Simone A, Laffan MA, McKinnon TAJ. Blocking von Willebrand factor free thiols inhibits binding to collagen under high and pathological shear stress. *J Thromb Haemost*. 2021;19:358–69.

[20] Passam F, Chiu J, Ju L, Pijning A, Jahan Z, Mor-Cohen R, Yeheskel A, Kolšek K, Thärichen L, Aponte-Santamaría C, Gräter F, Hogg PJ. Mechano-redox control of integrin de-adhesion. *Elife*. 2018;7:e34843.

[21] Butera D, Hogg PJ. Fibrinogen function achieved through multiple covalent states. *Nat Commun*. 2020;11:5468.

[22] Dong X, Leksa NC, Chhabra ES, Arndt JW, Lu Q, Knockenhauer KE, Peters RT, Springer TA. The von Willebrand factor D′D3 assembly and structural principles for factor VIII binding and concatemer biogenesis. *Blood*. 2019;133:1523–33.

[23] Javitt G, Fass D. Helical self-assembly of a mucin segment suggests an evolutionary origin for von Willebrand factor tubules. *Proc Natl Acad Sci U S A*. 2022;119:e2116790119.

[24] Ruggeri ZM, Mendolicchio GL. Adhesion mechanisms in platelet function. *Circ Res*. 2007;100:1673–85.

[25] Chen PC, Kutzki F, Mojzisch A, Simon B, Xu ER, Aponte-Santamaría C, Horny K, Jeffries C, Schneppenheim R, Wilmanns M, Brehm MA, Gräter F, Hennig J. Structure and dynamics of the von Willebrand Factor C6 domain. *J Struct Biol*. 2022;214:107923.

[26] Zhou YF, Springer TA. Highly reinforced structure of a C-terminal dimerization domain in von Willebrand factor. *Blood*. 2014;123:1785–93.

[27] Franz F, Daday C, Gräter F. Advances in molecular simulations of protein mechanical properties and function. *Curr Opin Struct Biol*. 2020;61:132–8.

[28] Rico F, Russek A, González L, Grubmüller H, Scheuring S. Heterogeneous and rate-dependent streptavidin–biotin unbinding revealed by high-speed force spectroscopy and atomistic simulations. *Proc Natl Acad Sci U S A*. 2019;116:6594–601.

[29] Gruber S, Löf A, Hausch A, Kutzki F, Jöhr R, Obser T, König G, Schneppenheim R, Aponte-Santamaría C, Gräter F, Brehm MA, Benoit M, Lipfert J. A conformational transition of the D′D3 domain primes von Willebrand factor for multimerization. *Blood Adv*. 2022;6:5198–209.

[30] Abraham MJ, Murtola T, Schulz R, Páll S, Smith JC, Hess B, Lindahl E. GROMACS: high performance molecular simulations through multi-level parallelism from laptops to supercomputers. *SoftwareX*. 2015;1-2:19–25.

[31] Hess B, Bekker H, Berendsen HJC, Fraaije JGEM. Lincs: a linear constraint solver for molecular simulations. *J Comput Chem*. 1997;18:1463–72.

[32] Miyamoto S, Kollman PA. Settle: an analytical version of the SHAKE and RATTLE algorithm for rigid water models. *J Comput Chem*. 1992;13:952–62.

[33] Páll S, Hess B. A flexible algorithm for calculating pair interactions on SIMD architectures. *Comput Phys Commun*. 2013;184:2641–50.

[34] Darden T, York D, Pedersen L. Particle mesh Ewald: an N ·log(N) method for Ewald sums in large systems. *J Chem Phys*. 1993;98:10089–92.

[35] Essmann U, Perera L, Berkowitz ML, Darden T, Lee H, Pedersen LG. A smooth particle mesh Ewald method. *J Chem Phys*. 1995;103:8577–93.

[36] Berendsen HJC, Postma JPM, van Gunsteren WF, DiNola A, Haak JR. Molecular dynamics with coupling to an external bath. *J Chem Phys*. 1984;81:3684–90.

[37] Bussi G, Donadio D, Parrinello M. Canonical sampling through velocity rescaling. *J Chem Phys*. 2007;126:014101.

[38] Parrinello M, Rahman A. Polymorphic transitions in single crystals: a new molecular dynamics method. *J Appl Phys*. 1981;52:7182–90.

[39] Lindorff-Larsen K, Piana S, Palmo K, Maragakis P, Klepeis JL, Dror RO, Shaw DE. Improved side-chain torsion potentials for the Amber ff99SB protein force field. *Proteins*. 2010;78:1950–8.

[40] Aliev AE, Kulke M, Khaneja HS, Chudasama V, Sheppard TD, Lanigan RM. Motional timescale predictions by molecular dynamics simulations: case study using proline and hydroxyproline sidechain dynamics. *Proteins*. 2014;82:195–215.

[41] Jorgensen WL, Chandrasekhar J, Madura JD, Impey RW, Klein ML. Comparison of simple potential functions for simulating liquid water. *J Chem Phys*. 1983;79:926–35.

[42] Zięba A, Ramza P. Standard deviation of the mean of autocorrelated observations estimated with the use of the autocorrelation function estimated from the data. *Metrol Meas Syst*. 2011;18:529–42.

[43] Chiu J, Wong JWH, Gerometta M, Hogg PJ. Mechanism of dimerization of a recombinant mature vascular endothelial growth factor C. *Biochemistry*. 2014;53:7–9.

[44] Cook KM, McNeil HP, Hogg PJ. Allosteric control of βII-tryptase by a redox active disulfide bond. *J Biol Chem*. 2013;288:34920–9.

[45] Chiu J, Tillett D, Dawes IW, March PE. Site-directed, ligase-independent mutagenesis (SLIM) for highly efficient mutagenesis of plasmids greater than 8kb. *J Microbiol Methods*. 2008;73:195–8.

[46] Jumper J, Evans R, Pritzel A, Green T, Figurnov M, Ronneberger O, Tunyasuvunakool K, Bates R, Zídek A, Potapenko A, Bridgland A, Meyer C, Kohl SAA, Ballard AJ, Cowie A, Romera-Paredes B, Nikolov S, Jain R, Adler J, Back T, et al. Highly accurate protein structure prediction with AlphaFold. *Nature*. 2021;596:583–9.

[47] Bryant P, Pozzati G, Elofsson A. Improved prediction of protein-protein interactions using AlphaFold2. *Nat Commun*. 2022;13:1265.

[48] Gaus M, Cui Q, Elstner M. DFTB3: extension of the self-consistent-charge density-functional tight-binding method (SCC-DFTB). *J Chem Theory Comput*. 2012;7:931–48.

[49] Gaus M, Goez A, Elstner M. Parametrization and benchmark of DFTB3 for organic molecules. *J Chem Theory Comput*. 2013;9:338–54.

[50] Putzu M, Gräter F, Elstner M, Kubař T. On the mechanism of spontaneous thiol-disulfide exchange in proteins. *Phys Chem Chem Phys*. 2018;20:16222–30.

[51] Gómez-Flores CL, Maag D, Kansari M, Vuong VQ, Irle S, Gräter F, Kubař T, Elstner M. Accurate free energies for complex condensed-phase reactions using an artificial neural network corrected DFTB/MM methodology. *J Chem Theory Comput*. 2022;18:1213–26.

[52] Maag D, Putzu M, Gómez-Flores CL, Gräter F, Elstner M, Kubař T. Electrostatic interactions contribute to the control of intramolecular thiol–disulfide isomerization in a protein. *Phys Chem Chem Phys*. 2021;23:26366–75.

[53] Tribello GA, Bonomi M, Branduardi D, Camilloni C, Bussi G. PLUMED 2: new feathers for an old bird. *Comput Phys Commun.* 2014;185:604–13.

[54] Aradi B, Hourahine B, Frauenheim T. DFTB+, a sparse matrix-based implementation of the DFTB method. *J Phys Chem A.* 2007;111:5678–84.

[55] Leontyev I, Stuchebrukhov A. Accounting for electronic polarization in non-polarizable force fields. *Phys Chem Chem Phys.* 2011;13:2613–26.

[56] Kirby BJ, Jungwirth P. Charge scaling manifesto: a way of reconciling the inherently macroscopic and microscopic natures of molecular simulations. *J Phys Chem Lett.* 2019;10:7531–6.

[57] Laio A, Parrinello M. Escaping free-energy minima. *Proc Natl Acad Sci U S A.* 2002;99:12562–6.

[58] Barducci A, Bussi G, Parrinello M. Well-tempered metadynamics: a smoothly converging and tunable free-energy method. *Phys Rev Lett.* 2008;100:020603.

[59] Raiteri P, Laio A, Gervasio FL, Micheletti C, Parrinello M. Efficient reconstruction of complex free energy landscapes by multiple walkers metadynamics. *J Phys Chem B.* 2006;110:3533–9.

[60] Fu H, Jiang Y, Wong WP, Springer TA. Single-molecule imaging of von Willebrand factor reveals tension-dependent self-association. *Blood.* 2021;138:2425–34.

[61] Zhu J, Choi WS, McCoy JG, Negri A, Zhu J, Naini S, Li J, Shen M, Huang W, Bougie D, Rasmussen M, Aster R, Thomas CJ, Filizola M, Springer TA, Coller BS. Structure-guided design of a high-affinity platelet integrin αIIbβ3 receptor antagonist that disrupts Mg^{2+} binding to the MIDAS. *Sci Transl Med.* 2012;4:125ra32.

[62] Kolšek K, Aponte-Santamaría C, Gräter F. Accessibility explains preferred thiol-disulfide isomerization in a protein domain. *Sci Rep.* 2017;7:9858.

[63] Hantgan RR, Stahle MC, Lord ST. Dynamic regulation of fibrinogen: integrin αIIbβ3 binding. *Biochemistry.* 2010;49:9217–25.

[64] Fu X, Chen J, Gallagher R, Zheng Y, Chung DW, López JA. Shear stress-induced unfolding of VWF accelerates oxidation of key methionine residues in the A1A2A3 region. *Blood.* 2011;118:5283–91.

[65] Tsai R, Interlandi G. Oxidation shuts down an auto-inhibitory mechanism of von Willebrand factor. *Proteins.* 2021;89:731–41.

[66] Chen H, Fallah MA, Huck V, Angerer JI, Reininger AJ, Schneider SW, Schneider MF, Alexander-Katz A. Blood-clotting-inspired reversible polymer–colloid composite assembly in flow. *Nat Commun.* 2013;4:1333.

[67] Tischer A, Madde P, Blancas-Mejia LM, Auton M. A molten globule intermediate of the von Willebrand factor a1 domain firmly tethers platelets under shear flow. *Proteins.* 2014;82:867–78.

[68] Wiita AP, Ainavarapu SRK, Huang HH, Fernandez JM. Force-dependent chemical kinetics of disulfide bond reduction observed with single-molecule techniques. *Proc Natl Acad Sci U S A.* 2006;103:7222–7.

[69] Li W, Gräter F. Atomistic evidence of how force dynamically regulates thiol/disulfide exchange. *J Am Chem Soc.* 2010;132:16790–5.

[70] Jordan PA, Gibbins JM. Extracellular disulfide exchange and the regulation of cellular function. *Antioxid Redox Signal.* 2006;8:312–24.

[71] Camacho CJ, Thirumalai D. Theoretical predictions of folding pathways by using the proximity rule, with applications to bovine pancreatic trypsin inhibitor. *Proc Natl Acad Sci U S A.* 1995;92:1277–81.

[72] Camacho CJ, Thirumalai D. Modeling the role of disulfide bonds in protein folding: entropic barriers and pathways. *Proteins.* 1995;22:27–40.

[73] Qin M, Wang W, Thirumalai D. Protein folding guides disulfide bond formation. *Proc Natl Acad Sci U S A.* 2015;112:11241–6.

[74] Zhu J, Zhu J, Springer TA. Complete integrin headpiece opening in eight steps. *J Cell Biol.* 2013;201:1053–68.

[75] Zhou YF, Eng ET, Nishida N, Lu C, Walz T, Springer TA. A pH-regulated dimeric bouquet in the structure of von Willebrand factor. *EMBO J.* 2011;30:4098–111.